2 Analytical Ultracentrifugation, Instrumentation

Centrifugation is a common technical process for the separation of materials consisting of two (or more) compounds having different sizes and/or showing different densities, such as dissolved macromolecules in a solvent or dispersed particles in a liquid. A centrifuge is basically an apparatus to create centrifugal fields by fast rotation of a rotor. The special design of centrifuges allows us letting these fields act on samples inside the rotor, which leads to a sedimentation (or flotation) of the dissolved/dispersed macromolecules/particles and also to their fractionation, if the macromolecules/particles are different in size and/or density. There is no clear definition from which magnitude of the centrifugal field on a centrifuge is called an *ultra*centrifuge. Usually, centrifuges that create fields higher than 5000 times the acceleration due to the Earth's gravitational field (g) are called ultracentrifuges [1].

An *analytical* ultracentrifuge, in turn, is an ultracentrifuge with one or several optical detection systems, which allow the observation of the fractionation process while the sample is centrifuged.

An analytical ultracentrifuge consists of different main components, namely, the centrifuge housing (see Sect. 2.1 and part 2.1 in Fig. 2.1) itself (including motor bearing, rotor axle/drive, safety vacuum chamber, temperature control, velocity control), the analytical rotor (see 2.2), one or several sample cells (including housing) inside the rotor (see 2.3), the optical detector unit (see 2.4), and a multiplexer unit if several measuring cells have to be detected simultaneously in the same experimental run (see 2.5). Figure 2.1 serves as guide to the structure of this Chap. 2.

While writing about instrumentation, it must be emphasized that the AUC bears considerable danger. The involved powers are enormous (for illustrative pictures of an accident with a preparative ultracentrifuge in 1998, see [2]). A lot of engineering has therefore been put into the development of proper safety elements. For example, the centrifuges are equipped with a system to prevent the rotor from

(i) oscillations created by imbalance at the start of the run or during the run, e.g., if a window breaks, and
(ii) being run with overspeed.

This overspeed control is particularly important, as the typical rotor would explode if speeded up to about 120 000 rpm, or more. For the case of explosion, the rotor itself is surrounded by a safety chamber of heavy steel.

In this chapter, the most important components of analytical ultracentrifuges are described. We will concentrate on state-of-the-art instrumentation, and we

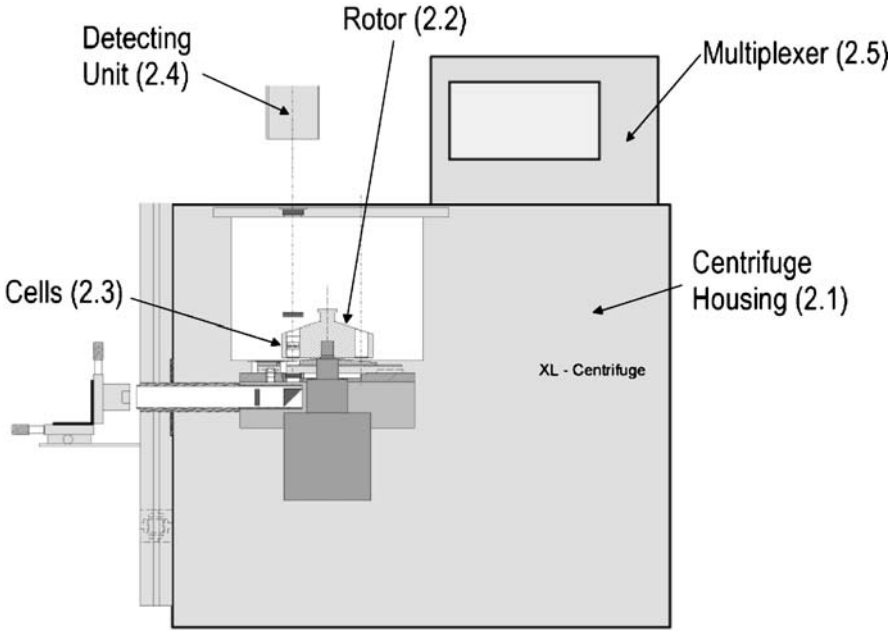

Fig. 2.1. Schematic picture of an analytical ultracentrifuge and its most important components

will therefore leave out most of the historically relevant aspects. For the latter, the reader is referred to [3] or [4].

2.1 Ultracentrifuges

It has been a long way from the room-filling, user-made, really efficient first analytical ultracentrifuge in Uppsala developed by Svedberg and coworkers in the 1930s, to the desk-sized compact, ready-to-use machines of the early 1990s, such as the Beckman Optima XL-A.

Starting with mainly homemade individual items in the early days of analytical ultracentrifugation, the development has subsequently been driven by different companies including Beckman, Phywe, Christ (Heraeus), Metrimpex (MOM), Hitachi, MSE, and Sorvall. Still, all these companies, with the exception of Beckman-Coulter, gave up the production of AUCs and are producing only preparative ultracentrifuges today.

So, nowadays, basically two types of analytical ultracentrifuges are playing a role in the scientific community:

(i) the commercially available Beckman-Coulter AUC (Optima XL-A/I), and
(ii) user-made analytical ultracentrifuges, created mostly as modifications of the commercially available preparative ultracentrifuges.

The present instrument of Beckman-Coulter is the Optima XL-A/I. This is the follow-up model of the perhaps most successful AUC apparatus (in terms of numbers of distributed machines), the famous Model E, which was already equipped with a UV scanner, six-cell multiplexer, interference and Schlieren optics with photographic detection. The modern Optima XL-A/I series was released in 1990/1997, inducing a renaissance of the analytical ultracentrifugation technique in general. The integration of modern computer technology, the more compact design, a higher safety standard, a better electrical drive, a better temperature control of the apparatus, the introduction of a CCD camera, and the online digitization of the measuring data transformed the whole measurement procedure into a more user-friendly and easy-forward process, allowing even non-specialists to perform experiments to a certain degree. However, analytical ultracentrifugation is still not a black-box method, and will probably never become one.

2.1.1 The Beckman-Coulter Optima XL-A/I

The Optima XL-A/I series (see Fig. 2.2) offers two modern, independent optical systems – the UV/Vis absorption optics (since 1990), and the Rayleigh interference optics (since 1997). In contrast to the precursor Model E, unfortunately no Schlieren optical system is integrated. The different optical systems will be described below.

Depending on the rotor, speeds up to 60 000 rpm can be obtained. This corresponds to gravitational fields of over 290 000 times the Earth's gravitational field g (to give an idea of the huge forces the AUC deals with: a mass weighing one gram in real would weigh 290 kg inside the centrifuge or, in other words, a person of 70 kg would weigh 20 000 t inside such a centrifugal field). The relative gravitational field or, as it is often referred to, the relative centrifugal field (RCF), can easily be calculated according to the following simple equation (2.1):

$$\mathrm{RCF} = \frac{r \cdot \omega^2}{g} \tag{2.1}$$

with the angular velocity ω (in rad/s), the radius r (that is, the distance from the axis of rotation, 5.7 – 7.2 cm in the XL-A/I), and the Earth's gravitational field g ($1g \approx 9.81\,\mathrm{m/s^2}$).

Additionally, on the top of the Optima XL-A/I, Fig. 2.2 shows an analytical eight-cell rotor and some measuring cells.

Temperature Control of the Optima XL-A/I

Exact control of the temperature is essential to any thermodynamic measurement, and control within 0.5 K, or better, has to be guaranteed. Svedberg's first AUC contained a safety chamber that was continuously flooded with gaseous hydrogen to create small drag, and to allow control of the temperature within the chamber. In later developments, the rotor-containing safety chamber was evacuated to guarantee the smallest possible air-friction resistance to the rotor's movement, thus eliminating rotor heating by air friction.

Fig. 2.2. Modern analytical ultracentrifuge Optima XL-A/I produced by Beckman-Coulter

In the former Beckman Model E, cooling of the chamber was achieved by water cooling of a cladding surrounding the rotor inside the chamber. The heating elements were different from these, and were located at the chamber bottom. This led to temperature gradients within the chamber, and therefore within the rotor itself. The temperature was measured in a very specific way: a needle was fixed to the bottom of the hanging analytical rotor, and a temperature-dependent electrical resistance was installed inside the rotor. This needle dipped into a mercury bath, thus closing an electrical circuit. By measuring the heat resistance in this electrical circuit, the rotor temperature was estimated.

In the modern XL-A/I, the vacuum chamber is heated and cooled via Peltier elements located in the aluminum heat sink at the bottom of the chamber, which leads to a homogeneous temperature throughout the vacuum chamber via heat exchange by radiation. The temperature is measured contact-free at the bottom of the rotor via an IR detector, which, of course, requires the rotors to be black-colored. The temperature range covered by the instrument is 0 – 40 °C, according to biochemical needs. Next to the technical problems, physics also complicates the exact control of temperature. Due to adiabatic cooling occurring when the

rotor is speeded up to high angular velocities, the temperature in the rotor may vary by 0.1 – 0.3 K. Hence, in high-speed runs, first data collections should not be performed before 10 – 15 min after reaching a constant final speed. This guarantees that heat exchange has reached equilibrium.

Drive and Velocity Control of the Optima XL-A/I (Compared with the Model E) As well as the exact knowledge of temperature, the exact angular speed $\omega = 2\pi N$ or the running time integral $\int \omega^2 \, dt$, in the case of applying sweeping $\omega(t)$ techniques (see Chap. 3), of the rotor must be determined. It was shown [5] that, in the case of polymeric particles analyzed by applying turbidity optics, the results of the sedimentation analysis were independent of the velocity profile $\omega(t)$. That was due to the exact knowledge and continuous recording of $\int \omega^2 \, dt$. It has to be kept in mind that the angular velocity ω is squared in (1.5) for the determination of the sedimentation coefficients.

In the former Beckman Model E, the electrical drive motor was coupled for safety reasons to the rotor drive shaft via a 1:7 mechanical speed transformation unit. The rotor was linked to the drive shaft by hanging on a steel filament (i.e., the rotor axle) that was only 2 mm in diameter. Sometimes, this 2-mm axle broke, and the rotor fell down within the safety chamber. This Model E configuration allowed the operation of the centrifuge at certain fixed rotor speeds only. The speed was measured indirectly in the drive.

Today, in a safer manner, the rotor of the XL-A/I is put directly onto the drive shaft, which in turn is directly run by an electrical induction motor. The motor operates under computer control, and offers the user an infinitely variable regulation of the speed. The actual velocity ω is measured optically via a stroboscopic ring fixed onto the rotor bottom, which is read out by a photoelectric relay. This ensures that the rotors are not overspeeded, which could lead to rotor explosion, as pointed out above. Another special unit integrated into the drive dampens the rotor oscillations at some critical rotor speeds around 1000 rpm, as well as rotor oscillations created by imbalance. It will stop the rotor if the imbalance is too high. In contrast to the former Model E, the rotor in the XL-A/I is standing on the drive shaft. The driving axle is flexible in such a way that the angle between the rotor axis and motor axis (which is fixed to the vacuum chamber and laboratory floor) can change with rotor velocity. The system is self-stabilizing, like a gyroscope (indeed, it is a gyroscope!), and very safe.

2.1.2 User-Made Centrifuges

Considering that Beckman-Coulter is a more biochemically oriented company, and because most applications of AUC originate from biochemical questions, the design of their last analytical ultracentrifuges, the Optima XL-A/I, is driven by the corresponding requirements. As mentioned above, this book mainly concentrates on the application of the AUC in the research on synthetic polymers and colloids. In this field, we encounter special requirements that are not fulfilled by the XL-A/I. To give only three examples:

(i) Far more than in biochemical applications, the sedimentation velocity experiment is the central experiment type. The colloidal particles or polymers examined are often "large" compared to typical biochemical samples, and therefore sediment much faster. Thus, the need to create fast detectors and variability of rotor speed arises, because a precise and permanent measurement of the running time integral $\int \omega^2 \, dt$ has to be ensured.
(ii) In contrast to biological samples, synthetic polymers and colloids frequently exhibit turbid samples, sometimes in the visible range. Hence, a fast turbidity (= light scattering) detector is important to measure particle size distributions.
(iii) Biological samples are usually measured at the smallest possible concentration in order to obtain physical information on single molecules, or aggregates consisting of a relatively low number of molecules. In contrast hereto, in colloidal systems the intermolecular or, more often, the inter-particle interactions at higher concentrations are of great importance. Very high concentration differences are also created in two-component density gradients, where often one component is not transparent for UV light. Hence, there is a demand for the universal Schlieren optics, which allows measuring high concentrations (up to 100 g/l) and steep refractive index gradients inside the cell.

In order to fulfill these specific and industrially important requirements for the fast detectors (and $\int \omega^2 \, dt$ estimation), turbidity detectors and Schlieren optics, some laboratories have made their own developments of AUC instrumentation. Using the preparative Beckman XL series as a basis for development, extensive modifications have been added (see [5–8] and [12]).

As example, in this section we first describe the modifications (see Fig. 2.3) added to the original Optima XL for the introduction of a new user-made digital Schlieren optical setup [7, 8]. Later, in Sect. 2.4.4, we describe two other modifications: Laue's fluorescence detector [12], and a BASF-made turbidity detector [5] to measure precise particle size distributions (see also Sect. 3.5.1).

Figure 2.3 shows the most important modifications for introduction of Schlieren optics into an Optima XL:

- An optical bench containing the light source (1) and Schlieren slit assembly (2) has been mounted to the left side of the XL housing. The flash lamp is adjustable by an x–y–z stage.
- A horizontal hole is drilled into the heat sink (6), which is fixed with the motor (5) and an optical tube containing the collimating lens (3) and the 90°-deflection prism (4) is added.
- For completion of the optical path through the rotor (8), the vacuum chamber (10) has been modified by drilling in two vertical holes, one into the heat sink and the other into the moveable cover plate, that allow the mounting of vacuum-sealed windows (7). For adding a rack that carries the condensing lens (9), existing thread holes in the heat sink are used.

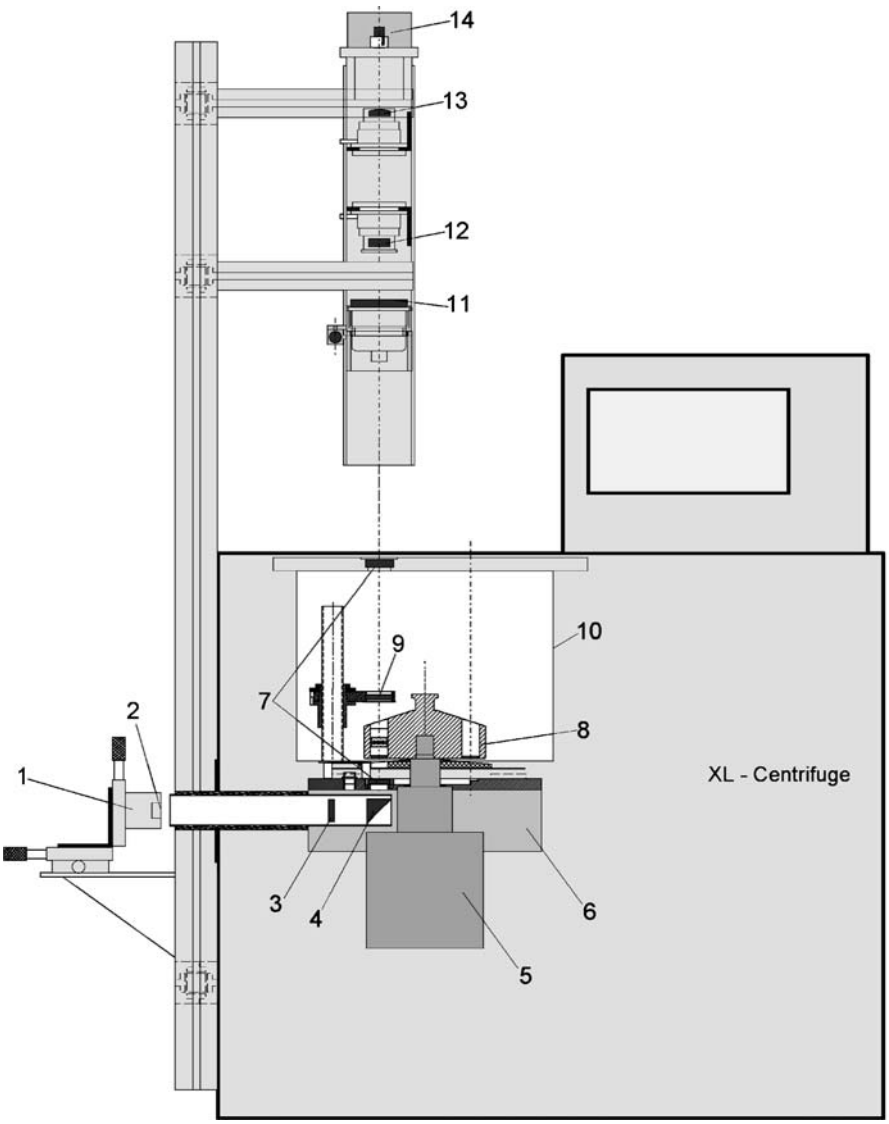

Fig. 2.3. Modifications of an Optima XL with Schlieren optics (and a multiplexer; reprinted with permission from [8])

- A charge-coupled device (CCD) camera (14) was applied as detecting unit. The CCD camera, and the remaining optical elements of the Schlieren optics, i.e., the phase plate (11), camera lens (12), and cylindrical lens (13), are mounted to a scaffold above the vacuum chamber, as indicated in Fig. 2.3.
- Independent from the Optima XL velocity control, a user-made velocity control system to trigger the flash lamp has been implemented (thus, the safety system

of the original XL, especially over speed and imbalance control, is not changed). By polishing a narrow strip of the rotor bottom, a reflecting mirror was created, and a light barrier has been added to the heat sink under the rotor. This allows us to generate one, single narrow light pulse per revolution that is converted to an electrical signal that, in turn, is applied to measure the exact velocity of the rotor and to trigger the light source of
the Schlieren optics. The trigger device is able to trigger not only one measuring cell. In the multiplexer state, it is possible to trigger each single cell of the eight cells measured simultaneously, thus allowing Schlieren optical *superimposition* of one cell with any other cell. The superimposition of the measuring cell with the reference cell is chosen as the standard.

Figure 2.4 shows a picture of the physical Schlieren optics multiplexer setup as realized in the AUC laboratory of BASF.

Fig. 2.4. Photograph of the physical Schlieren optics multiplexer setup of a modified Optima XL realized in the AUC laboratory at BASF

2.2 Rotors

In the early days of centrifugation, a lot of work was spent on the design of analytical rotors. Whereas in earlier days steel and later aluminum were the predominately used material, nowadays almost exclusively titanium rotors are applied.

The analytical rotors are built from one piece of titanium. Depending on the rotor type, four or eight holes are drilled into the titanium, leading to four- or eight-hole rotors (see Fig. 2.5). The distances between the midpoints of the holes and the axis of rotation are $r = 6.50\,\text{cm}$. Usually, one of the holes is loaded with a reference cell (also called counterbalance), which contains two radius reference marks at the positions of $r = 5.70$ and $7.20\,\text{cm}$. The reference cell is used to perform the radial calibration at given centrifugal speed. The remaining holes carry up to seven different measurement cells, which in turn can contain up to eight different samples each if multi-channel cells are used. For safety reasons, it is important to know the allowed maximum speed for the different types of rotors. The most frequently used, commercially available analytical rotors have maximum speeds of 50 000 and 60 000 rpm. The lifetime of rotors depends on the time period they have been rotated at maximum speed. If the revolution speed during the experiment is restricted to 95% of the allowed maximum rotor speed, then the lifetime of rotors is nearly unlimited. Compared to the former Model E, the new Beckman Optima XL-A/I is run only with redesigned titanium rotors. The stress levels throughout the rotors are more uniform, and the rotors are lighter. This leads to a more uniform adiabatic temperature change (cooling) while the rotor is accelerated. For every rotor and every run, a continuous running lifetime check protocol has to be written, recording actual running speed and total running time. This is done inside the PC of the XL-A/I automatically for safety reasons.

Fig. 2.5. Eight-hole analytical rotor made of titanium by Beckman-Coulter

2.3 Measuring Cells

The part of an analytical ultracentrifugation system that is in direct contact to the sample is the measuring cell. The cell consists of many pieces. Figure 2.6 shows the cell assembly of a typical analytical ultracentrifugation cell. Characteristically, all these pieces must work under extremely high mechanical stress at maximum rotor speed.

AUC cells must fulfill at least two criteria:

- They should not leak or distort even at high centrifugal fields, which create very high hydrostatic pressures of up to 250 bar [9] at the bottom of the solution column.
- They should allow passage of light through the cell via stable quartz or sapphire windows while the rotor is spinning.

There is a big variety of ultracentrifugation cells available, depending on the kind of experiment they are used for. The differences occur mainly in the choice of the centerpiece, and that of the windows. Because of the high mechanical strength, the most common window materials are optically polished plan-parallel sapphire and quartz glass. The plates exhibit a thickness of 5 mm. It will be pointed out in the corresponding chapters which type of glass is preferably applied in the particular type of experiment. Generally, sapphire is the material of choice, if available. One advantage of quartz glasses is their lower price. Another advantage is the broader spectrum of light that can pass through quartz when UV detectors are applied.

Whereas it is very uncommon to create user-made rotors and other parts of the cell, the centerpieces of AUC cells are frequently built or modified by users in order to adapt them for their special needs. The centerpiece is the heart of an AUC measuring cell (see Fig. 2.7). It is made of aluminum, titanium, Kel-F, Teflon or charcoal/aluminum-filled Epon. In principle, there are four types of analytical ultracentrifugation centerpieces:

(i) The mono-sector centerpiece only contains the sample solution. It is mainly used with Schlieren optics and the turbidity detector.
(ii) The double-sector centerpiece has two separate chambers, one for the sample solution, the other for the solvent. It is used with all detecting systems (interference optics, UV/Vis absorption, and Schlieren optics).
(iii) Multi-channel centerpieces for 3 – 5 different samples can exhibit very different architectures (see Fig. 2.7c,f). In principle, they are double-sector centerpieces. They are applied exclusively in equilibrium runs (see Chap. 5).
(iv) Synthetic boundary centerpieces exist in two different types, the capillary type and the valve type (see Fig. 2.7d,e). They are designed to allow the layering of solvent (or solution) onto a sample solution (or solvent) while the rotor is spinning (see Chap. 3).

In most cases, the channels of the centerpieces are sector-shaped to prevent convection during sedimentation due to the radially sedimenting sample. The standard thickness of centerpieces is $a = 12$ mm. For special experimental designs, 1-, 2-, 3-

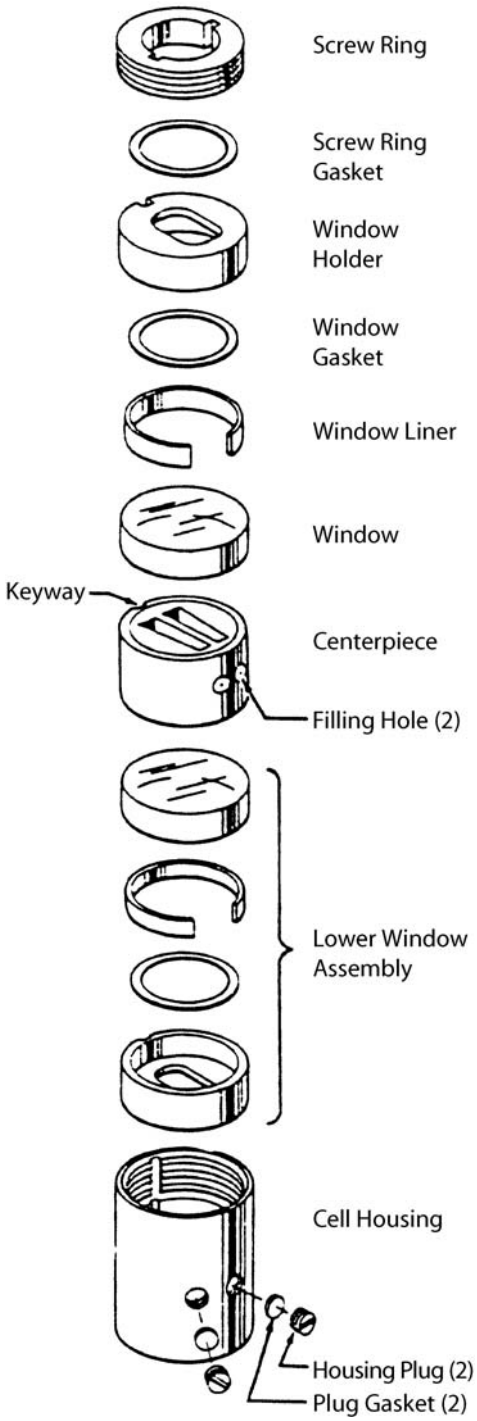

Fig. 2.6. Cell assembly with an (elastic) Kevlar double-sector centerpiece, which needs no gaskets between windows and centerpiece. In the case of (hard) metal centerpieces, two additional gaskets are required (reprinted with permission from [30])

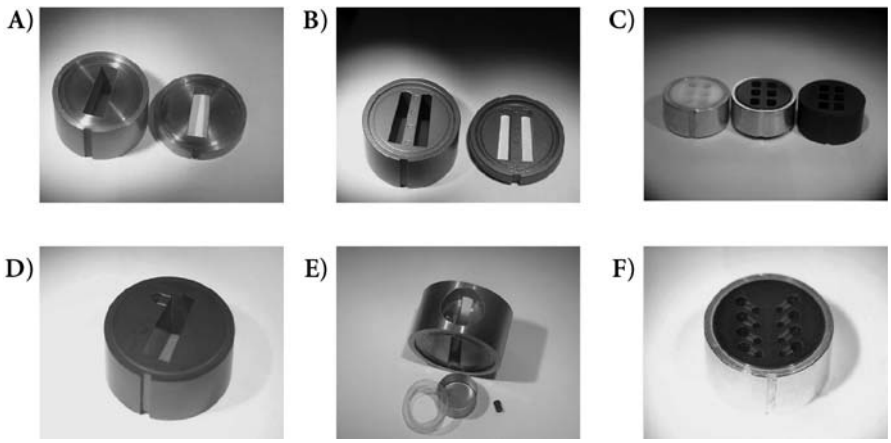

Fig. 2.7A–F. Some examples of different AUC centerpieces: **A** two mono-sector centerpieces (12 and 3 mm) made from aluminum, used for velocity runs applying Schlieren or turbidity optics; **B** two double-sector centerpieces (12 and 3 mm) made from aluminum, used for velocity and equilibrium runs applying interference, absorption or Schlieren optics; **C** three 12-mm multi-channel double-sector centerpieces (made from different materials) for sedimentation equilibrium experiments; in equilibrium experiments, the sector shape of the centerpiece holes/chambers can be omitted; **D** synthetic boundary 12-mm double-sector centerpiece of the capillary type; **E** synthetic boundary 12-mm single-sector centerpiece of the valve type with storage bin, rubber valve, and gasket; **F** multi-channel 12-mm double-sector centerpiece for the study of four solvent–solution pairs in sedimentation equilibriums runs

and 25-mm centerpieces have been developed and used. By varying the thickness of centerpieces, the layer thickness a of the sample in the optical path is varied as well. Depending on the applied detecting system, the concentration of the sample and the sample's optical properties, the optimum thickness may be different. Thus, the proper choice of the centerpiece is important when the experiment is designed. In Fig. 2.7, a selected assortment of different centerpieces for various purposes is given.

The design of the modern Beckman Optima XL-A/I series accommodates the continuous use of the existing cells of the preliminary Model E centrifuge (with exception of the 30-mm cell). Only small modifications have been added to XL-A/I cells, such as smaller window holders, different window material (quartz of higher purity), or anodized screw rings. Some of the most important parts of AUC cells in the case of metal centerpieces, such as aluminum or titanium, are flat elastic gaskets between the centerpieces and the two glass windows (mostly cut out of thin polyethylene foil). They have to tighten the cell, and to prevent leakage of the solutions. Furthermore, they have to diminish the mechanical stress onto the (brittle) windows (see Fig. 2.6). For elastic centerpieces, such as Kel-F, charcoal-filled Epon or Teflon, gaskets are not needed (that is the reason why they are not shown in Fig. 2.6; rather, only the similar gaskets between window and window holder are shown). To close the cell safely, the assembled cell has to be tightened with a torque wrench at defined torque.

The cells have to be inserted into the rotor in a correct manner to avoid convection. Adjusting the horizontal axis of the centerpieces is done by turning the cell inside the rotor hole until this axis is in exact alignment with the rotor axis, indicated by meeting of two marks. Furthermore, to avoid imbalance during the run, cells inserted in opposite holes of the rotor are adjusted to have the same weight (within a maximum difference of 0.5 g).

2.4 Detectors

The essential data collected from an AUC experiment are the radial concentration profile $c(r)$ of the examined sample in the cell at a given time t. The most common detectors make use of three properties of the dissolved or dispersed sample: specific light absorption, light scattering (turbidity), and light refraction. Therefore, different types of detection systems have been integrated into analytical ultracentrifuges. Roughly, they can be divided into three classes:

(i) Detector systems that allow one to obtain specific information on the chemical composition of the sample. The most important example from this class of detectors is the UV/Vis absorption optics integrated in modern XL-A/I analytical ultracentrifuges. Another detector of this type, the fluorescence detector, is recently commercially available. This class of detectors makes use of the sample's specific light absorption/fluorescence.

(ii) The light scattering or turbidity detector is also an absorption detector, but it is not dependent on the specific interaction of light with chemical groups of molecules at characteristic light wavelengths λ. Rather, it is a universal detector dependent on the size of the light scattering particle with respect to Mie's light scattering theory.

(iii) Detector systems that record the overall change of the concentration in the cell during centrifugation. Detectors of this type are interference optics (integrated in XL-A/I machines) and Schlieren optics. Both detectors can be applied whenever the examined dissolved solute particles exhibit different refractive indices compared to the solvent. Thus, this (universal) detector class makes use of the difference in light refraction Δn between the solution and solvent.

Detectors can also be classified as follows (see Figs. 2.8 – 2.13):

– Detectors that scan the cell radially (see Fig. 2.8d). The optical unit is moved stepwise along the radial axis of the cell, i.e., along the cell sectors. The step width is adjustable, and usually lies in the range 10 – 100 µm. At each radial position r, the optical information is recorded. The single measurements are then added to result in a radial concentration profile $c(r)$ of the cell at given time t. The most important example for a scanning type of detector is the UV/Vis absorption detector, as it is realized in the Optima XL-A, and the known fluorescence detectors. The scanning time has to be fast, compared

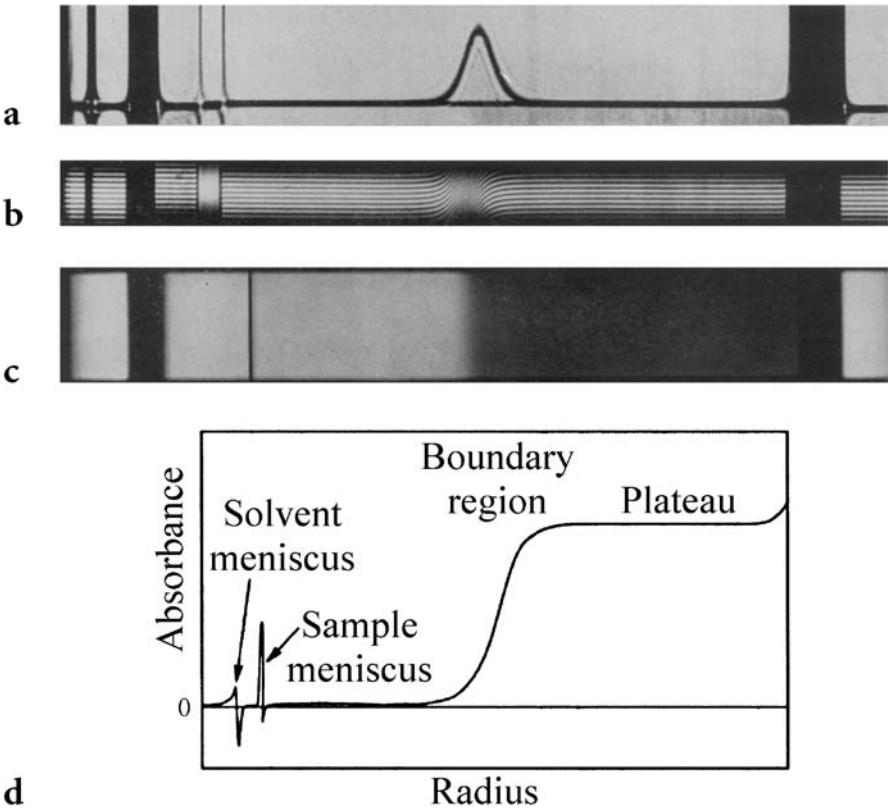

Fig. 2.8a–d. Typical optical patterns as derived by **a** Schlieren optics, **b** interference optics, **c** UV optics via photo-plates, and **d** UV optics via radial scanner (see also Fig. 5.1; reprinted with permission from [30])

to the sedimentation process observed by it. Otherwise, the assumption that the whole concentration profile was measured at once would lead to serious errors. In the case of the UV/Vis absorption optics, especially at low rotor speeds (approximately below 10 000 rpm), this is a real drawback of the XL-A. Scanning detectors are working well in equilibrium runs.

– Another detector type records the optical information at a given fixed radial position r as function of time t. The most important example of this type is the turbidity (= light scattering) detector, where the optical unit is located at the midpoint of the radial axis of the cell (see Fig. 2.13). Here, the change of intensity of the light I passing through the cell is recorded over the whole duration of the experiment, i.e., $I(t)$. The result is a single curve containing the whole experimental information.
– A third class of detectors records the whole concentration profile $c(r)$ at once at a given time t, without applying a scanning unit (see Fig. 2.8a–c). Representatives of this class are the interference and the Schlieren optical system,

where a light flash illuminates the whole cell at once. The result is a picture of the whole cell containing the concentration profile $c(r)$ at a given time t. The picture is recorded on a photo-plate or onto the chip of a CCD camera.

In the following sections (Sects. 2.4.1, 2.4.2 and 2.4.3), the three most important detecting systems – the absorption, the interference, and the Schlieren optical detectors – will be explained in detail.

Typical optical patterns obtained by the three main optical detecting systems are shown in Figs. 2.8 and 2.13 (see also Fig. 5.1). For an extensive description of these optical systems, see [10].

As mentioned above, only the Rayleigh interferometer as an online detector and the absorption optics are still available on modern ultracentrifuges (i.e., the XL-A/I). Few users adapted the Schlieren optics for use in the Beckman Optima XL. As a further detection system, a fluorescence detector was reported. This system is extremely sensitive, and allows the selective investigation of compounds with concentrations as low as 10 ng/ml, even in mixtures with a much larger amount of other components [11]. A prototype fluorescence detector for the Optima XL-A/I ultracentrifuges has recently been constructed, so that now a third detector is commercially available that can be simultaneously used in a modern analytical ultracentrifuge [12].

Amazingly, one of the most important detectors for use especially in industrial R&D is commercially not available: turbidity optics [13, 14]. A turbidity optical system is realized only in very few laboratories throughout the world. It is mainly used to determine particle size distributions. This detector is described at the end of this section. It will also be addressed in Chap. 3 due to its high relevance for particle sizing.

Generally, it is advantageous to combine several optical systems (= multiple detection). Especially the combination of the Rayleigh interference optics and the UV/Vis absorption optics can yield important information about complex systems, for example, when an absorbing component is selectively detected with the absorption optics, whereas the Rayleigh interferometer would detect all components together simultaneously [15, 16]. An example is given in Sect. 7.2 and Fig. 7.4.

2.4.1 Absorption Optics

The basis for applying absorption optics is well known from spectroscopy. Light passing through a solution containing light-absorbing molecules loses intensity in a specific way. The Lambert–Beer law (2.2) describes the interaction quantitatively:

$$A = \lg \frac{I_0}{I} = \varepsilon \cdot c \cdot a \tag{2.2}$$

with absorption A, intensity of light after passing the sample I, intensity of light passing the solvent-filled cell I_0, specific decadic absorption coefficient ε, the concentration of the sample c, and the thickness of the measuring cell along the optical path a.

Figure 2.9 shows the principal setup of the UV absorption optics as realized in the Beckman Optima XL-A/I. A xenon flash lamp with a nearly continuous light spectrum $190 < \lambda < 800\,\text{nm}$ is used as a light source. While the rotor (containing up to eight AUC cells) spins, the lamp is triggered to flash when the cell of interest passes the optical path. Therefore, this XL-A/I UV/Vis scanner is a multiplexer unit, too.

The triggering of the flash lamp is based on the exact measurement of the actual rotor speed. This is realized by a Hall-effect sensing device based on a magnet placed on the bottom of the rotor. Whenever the magnet passes the sensing device placed at the bottom of the vacuum chamber, the magnet induces an electrical signal. The position of the cell, and the sector of the cell of interest with respect to the position of the magnet on the rotor is known, and therefore the time delay from the magnet passing the sensing device until the lamp has to flash can be calculated within the XL-A/I computer, using the known rotor speed.

The duration of a single flash is about 2 – 3 µs, which is sufficient to create data from only one sector of the double-sector cell at once. With a maximum shot frequency of 100 Hz, the lamp can flash every ten revolutions at the maximum centrifugation speed of 60 000 rpm.

Light from the flash lamp passes an aperture (1 mm in diameter) to hit the diffraction grating of the monochromator at the top of the optical arm. Absorbing reflectors that hold back all disturbing light from other, unwanted wavelengths surround the grating. The grating itself is adjustable by high-precision electrical motor gears that allow the adjustment of the desired wavelength. The grating obeys a nominal band pass of 2 nm, and covers the wavelength range 200 – 800 nm. Because the flash intensity is not constant from flash to flash, for standardization the monochromatic light from the grating hits an 8% reflector. That means that 92% of the light passes the reflector while 8% is reflected onto the incident (= standardization) detector. The intensity value measured by this detector is needed to normalize these pulse-to-pulse variations in the light intensity of the xenon flash lamp. This procedure is necessary because one flash illuminates just one sector of a double-sector measuring cell. Below the 8% reflector, a second aperture prevents the illumination of any other, undesired sector of the measuring cell. The monochromatic light then leaves the optical arm, and passes through one of the sectors of the measuring cell containing either the sample or the corresponding solvent. By this optical setup, it is assured that the monochromatic light is parallel with respect to the normal projected onto the window surface of the measuring cell. While passing the measuring cell, the intensity of light is decreased by the interaction with the sample or solvent, according to (2.2), i.e., Lambert–Beer's law. Below the rotor, the remaining light passes to a moveable lens-slit assembly (see insert in Fig. 2.9) that fulfills certain functions:

– The aperture of the lens-slit assembly determines the radial resolution. The width of the slit is 25 µm. The lens-slit assembly moves stepwise as a unit driven by an electrical motor, and allows one to scan the sector of the measuring cell radially. The step width Δr can be adjusted with a smallest step width of 5 µm

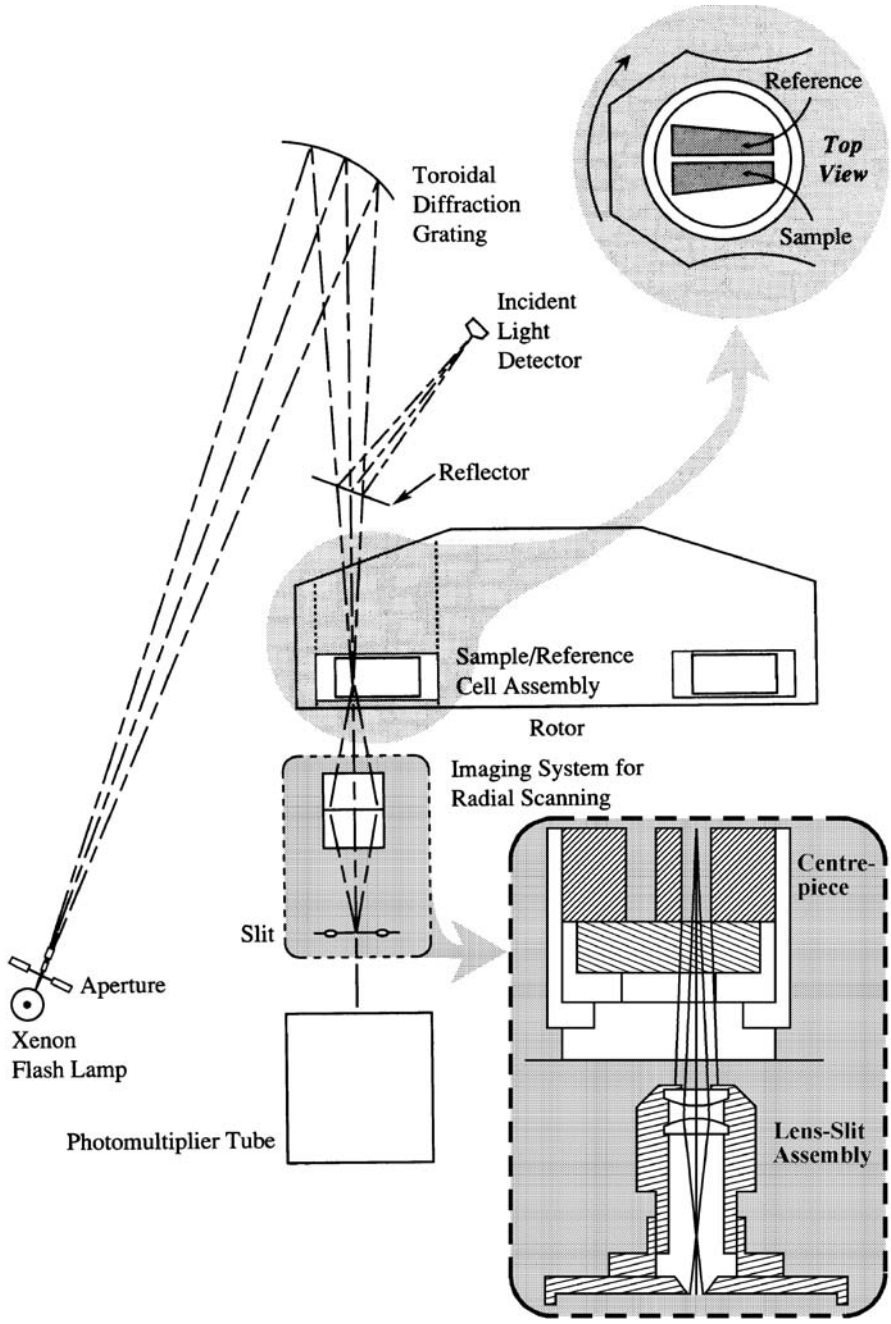

Fig. 2.9. Setup of the UV absorption optics of the Optima XL-A/I (reprinted with permission from [30])

steps. The lens focuses the light onto the photomultiplier (PM) tube, which measures the intensity I of light passing through the measuring cell.
- The camera lens of the lens-slit assembly creates an image of a slice at constant radius within the sector of interest of the measuring cell on the PM tube. A slice of constant radius contains redundant information, and can therefore be used to improve signal quality.
- Another aperture at the bottom of the lens-slit assembly reduces the stray light intensity once more.

The light leaving the lens-slit assembly hits the PM tube, which comprises a large active area that is sufficient to record the complete scanned picture of the cell. Therefore, the PM tube can be kept stationary.

The intensity of the solvent sector I_0, and the intensity of the sample sector I, both recorded on the PM tube, normalized with the intensity from the stationary incident detector, are combined to reveal the desired absorption signal $A(r) = \lg I_0/I$ of the sample, at the radius position r.

The main drawback of the XL-A/I UV/Vis optical system is the long duration of a measurement. Especially at low rotor speeds, such a stepwise radial scan along a single cell at one wavelength, but with, for example, ten replicates at each radial position in order to improve the signal-to-noise ratio, can last up to about 15 min. Nevertheless, for the monitoring of equilibrium runs, where enough time for recording is given, the UV/Vis absorption optics of the XL-A/I is appropriate. For the rapid recording of sedimentation runs, faster detectors like interference or turbidity detectors are mandatory. It is an advantage of the XL-A/I UV/Vis detector that, during an AUC run, complete UV/Vis spectra can be obtained at a constant radial position – although with a poor quality – yielding information on the chemical nature of the solute.

In applying the UV scanning device, it is recommended (i) to choose as wavelength λ the maximum of the absorption peak, and (ii) to select a sample concentration c for which $A < 1.5$ is valid, i.e., a concentration where Lambert–Beer's law (2.2) is fully valid and in the *linear* range. If one uses a λ outside of the maximum, within the flank of the peak, it might occur that small errors in the XL-A monochromator wavelength are increased, and that A is measured incorrectly.

Another problem caused by excessively high concentrations is the so-called Wiener skewing, arising from steep radial refractive index gradients within the cell. Light passing such gradients can be deviated so strongly that it does not reach the target of the PM tube ("black band"). However, if this Wiener skewing is not obviously manifested as a partial black band within the XL-A-UV scan, its effect on the interpretation of absorption gradients may be safely ignored (see [31]).

2.4.2 Interference Optics

The interference optics as realized in the Optima XL-A/I series of Beckman (see Fig. 2.10) is based on the principle of a Rayleigh interferometer [10, 17, 18]. This, in turn, makes use of the fact that the velocity of light depends on the refractive

index of the medium it passes through, i.e., the higher the refractive index of the medium, the lower the velocity of the light. That means that the (small) refractive index difference $\Delta n(r) = (n_{\text{solution}} - n_{\text{solvent}})$, which is proportional to the corresponding concentration $c(r)$ at this radius position, can be monitored very rapidly by interference optics. This is made visible in form of a vertical deviation of the originally parallel interference fringes behind a double (also called Rayleigh) slit (see insert in Fig. 2.10).

The (folded) interference optics as realized in the Optima XL-A/I applies a triggerable laser diode ($\lambda = 675\,\text{nm}$) above the rotor as light source. The monochromatic parallel light from the light source passes through two parallel Rayleigh slits (= double slit) above the measuring cell that allow the *simultaneous* illumination of the reference (= solvent) and the sample sector of the measuring cell. Light from the two Rayleigh slits creates an interference pattern of parallel light and dark fringes (see Fig. 2.8b and insert in Fig. 2.10) behind the cell in the plane of the condensing lens (= CCD camera sensor plane). The "disturbance" of the light by a medium of higher refractive index causes the position of the fringes to shift vertically proportional to the refractive index difference Δn, and thus proportional to c at the radial point of interest. This vertical shift of the interference fringes is counted in numbers $J(r)$ of fringes. Because $J \cdot \lambda = \Delta n \cdot a$ and $\Delta n = (\mathrm{d}n/\mathrm{d}c) \cdot c$, equation (2.3) is valid (with the thickness of the centerpiece a and the known specific refractive index increment $\mathrm{d}n/\mathrm{d}c$).

$$J(r) = \frac{a \cdot (\mathrm{d}n/\mathrm{d}c)}{\lambda} \cdot c(r) \tag{2.3}$$

where $J(r)$ is an absolute measure of the radial concentration distribution $c(r)$ within the AUC cell. This is valid only in the case of sedimentation runs, and synthetic boundary runs where left of the sedimenting boundary the concentration is zero, and so we know the zero fringe. That is not given in the case of equilibrium runs, where no boundary exists and the sample concentration $c(r_{\text{m}})$ at the meniscus position r_{m} is finite and unknown, like the absolute fringe number J_{m} at this position. Hence, only a *relative* fringe shift $\Delta J(r)$ with respect to the meniscus is measurable. Thus, only a relative concentration $\Delta c(r)$ can be determined, too. In Sect. 5.2 (equations (5.7) and (5.8)), it will be shown for the case of equilibrium runs how the mass conservation law can be utilized to calculate $J(r_{\text{m}})$ and $c(r_{\text{m}})$.

Again, the detecting system of the older Model E by Beckman served as basis for the development of the new XL-A/I interference optics [18, 19]. In comparison, major changes have been made to the light source and the detecting unit. The constantly burning mercury lamp as light source was replaced by a pulsed laser diode. A CCD camera replaced the photographic plate as detecting unit. Nevertheless, the major improvement was the implementation of a computer routine that allows the fast digitalization and a fast Fourier transform analysis of the fringes (first described by T.M. Laue in [11], page 63). These data are collected online. More recently, significant improvements have been realized by changing the CCD camera system to the next camera generation, especially with increased resolution.

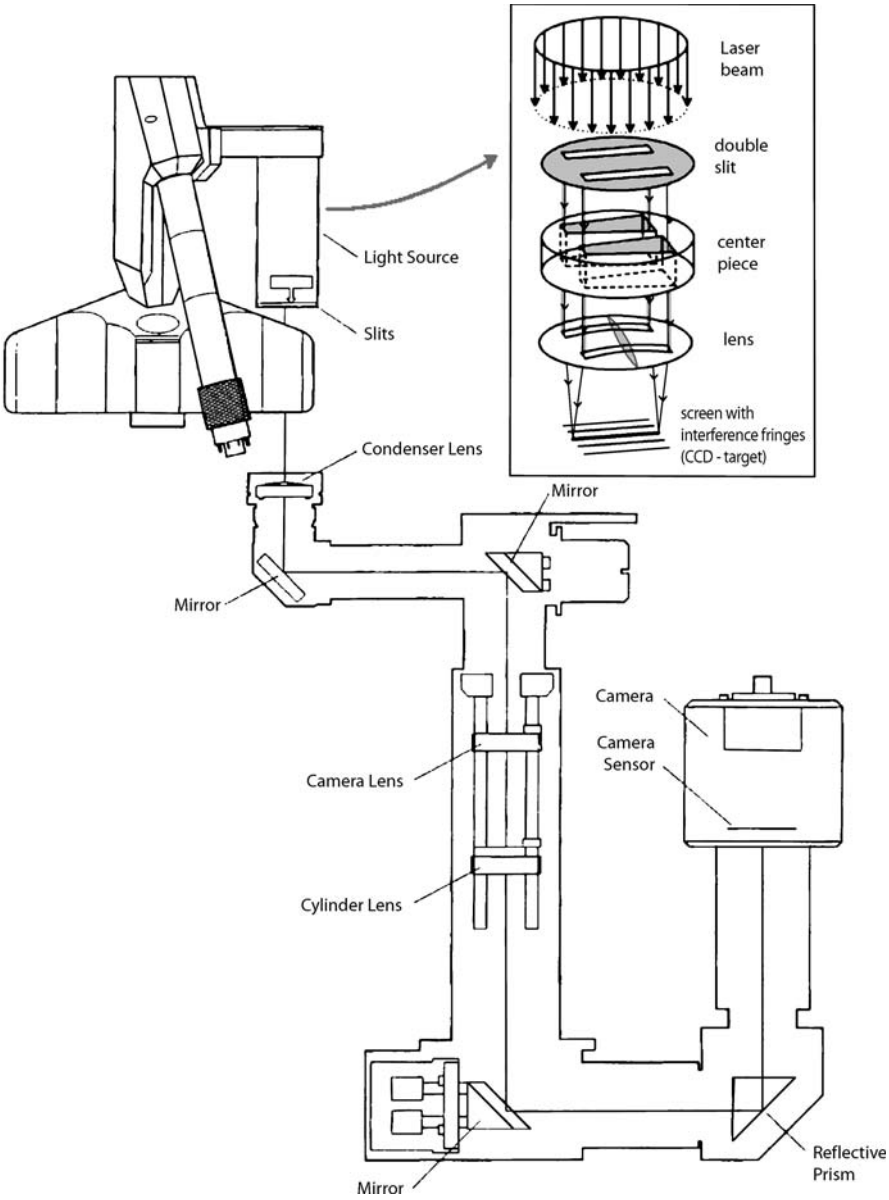

Fig. 2.10. Interference optics detector inside the Beckman Optima XL-A/I. The *insert* shows the principle of a Rayleigh interferometer with the interference fringes behind the double slit (reprinted with permission from [30])

Figures 3.1 and 3.2 show such a series of fast Fourier transform analysis fringes of the XL-A/I. All fringes are standardized on the (left) meniscus side to the same plateau position, $J = 0$. If one starts the fringe scan left of the meniscus,

sometimes one or more of the scans are shifted vertically by one or two integer numbers, for example, $\Delta J = \pm 1, \pm 2$, etc. However, this shifting can be corrected easily. Furthermore, if a sample shows too much turbidity, the fringes on the CCD camera monitor appear faintly, and it could be possible that the Fourier transform analysis fails.

2.4.3 Schlieren Optics

The Schlieren optics setup (as described above in Sect. 2.1.2 and Fig. 2.3) is similar to the setup of the Rayleigh interferometer but has a phase plate (or knife-edge) in the focus of the condenser lens as an additional element. As there is no commercially available system anymore, users are obliged to construct their own Schlieren optics, or transfer the Schlieren optics of an older Model E onto the Optima XL platform [7]. As mentioned above, the driving force to do this comes from some unique advantages of Schlieren optics, of which two are given here:

- It allows the use of simple mono-sector cells that are easy to handle, to tighten, and that assure highest reproducibility.
- Even steepest refractive index gradients (resulting often from steep density gradients) can be followed because these gradients can be compensated via wedge windows (as will be shown in Chap. 4, density gradients are among the most important experiments in AUC).

The modification of the preparative Optima XL centrifuge itself, especially the addition of a Schlieren optical system, has been outlined in Sect. 2.1.2. In this paragraph, only the necessary optical components will therefore be described.

The arrangement of the optical elements is basically as follows (see Fig. 2.3): the white light flash lamp (1) illuminates the Schlieren slit (2). Usually, a green filter (wavelength $\lambda = 546\,\mathrm{nm}$) between positions (7) and (11) is applied to create the light of a well-defined wavelength. The light then passes on through the collimating lens (3), a 90° glass prism (4), and then enters the vacuum chamber through a vacuum-sealed window (7). After passing the sample-containing cell inside the rotor (8), the light is focused by the condensing lens (9) through the second vacuum-sealed window (7) onto the plane of the phase plate (11). The new optical arm above the XL housing (see also Fig. 2.4) contains the camera lens (12) and the cylindrical lens (13). The light then falls onto the CCD camera (14) where the Schlieren picture is visible in form of a Schlieren peak or a Schlieren line on a TV monitor (see Fig. 2.8a). The CCD camera is connected to a computer for further image processing. In this arrangement, the light source is triggered mainly because of the high reliability of the stroboscopic light source, and the possibility to control the light source by newly developed multiplexer software. The ease to create superimposed pictures of more than one cell is another reason for triggering the light source. In each centrifugation run, there is one reference cell per rotor (also called counterbalance cell). This cell is used to perform radial calibration during centrifugation by superimposing the Schlieren picture of the reference cell and the Schlieren picture of the cell containing the samples examined. Figure 2.8a shows

such a superimposition. Furthermore, superimposition allows the measurement of up to seven different samples in one centrifugation run.

As one possible light source, a Cathodeon C 82007 xenon flash lamp (LOT/oriel, Darmstadt, Germany) can be used (flash frequency 0 – 100 Hz, flash energy 1 J). A CCD camera (for example, a digital black&white camera CCD 1300 from Vosskühler, Osnabrück, Germany, with a resolution of 1280 × 1024 pixels) serves as a detector unit.

Via a digital RS-644 interface, the camera is controllable by a computer. A Schlieren picture showing a typical Schlieren peak of a sedimentation velocity run is given in Fig. 2.8, in comparison with the results of interference and absorption optics delivered from the same sedimentation experiment (using a double-sector cell). In contrast to the interference optics, where the vertical fringe shift J is proportional to Δn and thus to the concentration c, in Schlieren optics the vertical shift of the Schlieren line is proportional to the radial refractive index gradient ($\mathrm{d}n/\mathrm{d}r$), and thus to the radial concentration gradient ($\mathrm{d}c/\mathrm{d}r$). In other words, integration of the Schlieren line ($\mathrm{d}n/\mathrm{d}r$) reveals redundant information with respect to one interference fringe $n(r)$, and vice versa (see also Fig. 5.1). Thus, the Schlieren peak area A_{schl} is proportional to the sample loading concentration c_0, and can be used to measure c_0 via (3.23). Continuous integration of the Schlieren peak, in combination with the law of conservation of mass, delivers the radial course of concentration $c(r)$ within the cell.

2.4.4 Other Detectors

Fluorescence Detectors

To our knowledge, two types of AUC fluorescence detectors are existing ([11] and [12]). Both are user-made. The latter one [12] is recently commercially available (albeit for a very high price). The manufacturer is Aviv Biochemical, Lakewood, NJ 08701. Thus, we give only a short description here. For more details, the literature or the manufacturers themselves should be consulted.

Especially for biochemical questions, a fluorescence detector is of high interest, mainly because of two inherent advantages:

- A fluorescence detector shows a sensitivity that has exceeded UV optics for decades. For example, Laue [12] performed equilibrium runs (see Fig. 5.12) and sedimentation velocity runs on the green fluorescent protein (GFP) with concentrations as low as $c = 0.012$ and 0.0024 g/l.
- A fluorescence detector can detect single components of a sample selectively, even if the component's concentration is very low compared to those of the other components of the sample.

The principle (see Fig. 2.11) is known from conventional fluorescence detectors: A laser is applied as a light source for the excitation of the fluorescence system. The light from the laser on a scanning stage passes optical elements that illuminate a very small Δr area of the sample sector (spatial resolution 60 µm, according to [11]). The response of the fluorescence system is detected either in

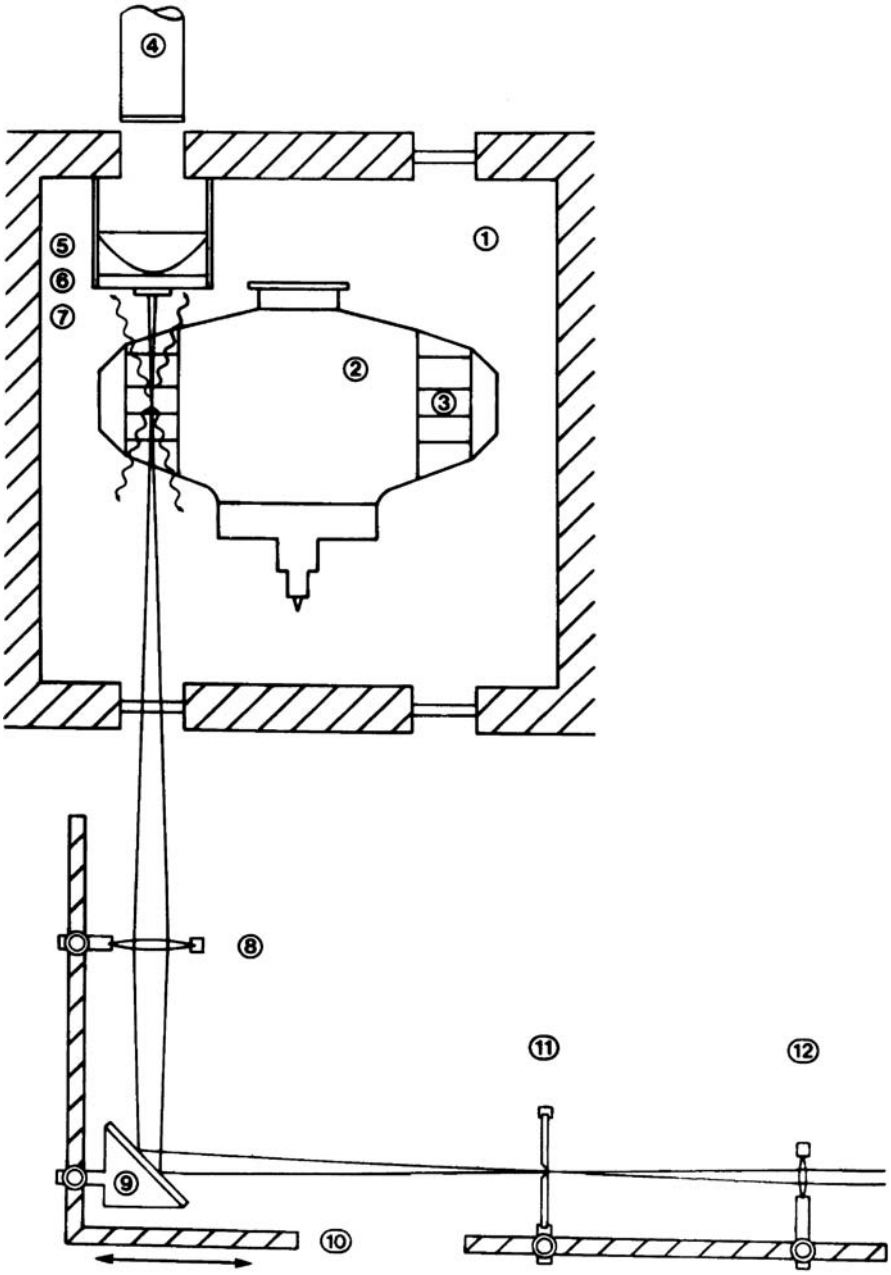

Fig. 2.11. Schematic setup of a user-made fluorescence detector realized by Riesner et al. [11] inside a Model E (reprinted with permission from [11])

reflectance [12] or in transmission mode [11] by a PM tube. A filter is used in front of the photomultiplier to ensure that only fluorescence light passes and excitation light is omitted.

Riesner et al. described the first fluorescence detector adapted to an AUC [11]. They used the geometry of the Schlieren optics channel of a Model E (see Fig. 2.11), and replaced the Model E components of the Schlieren optics by the components of the fluorescence detector. This allowed them to keep the instrumental changes of the Model E minimized, and to run the Model E–UV absorption detector simultaneously. A continuously running argon ion laser served as the light source, while a PM tube was applied to detect the florescence response of the system. Figure 2.11 shows a scheme of Riesner's setup with the filter (6) and the PM tube (4) above the rotor. In contrast, Laue [12] put his fluorescence detector into an Optima XL-A/I in a similar manner as described above for the case of Schlieren optics (Fig. 2.3). The small and compact detector (see Fig. 2.12) is directly installed within the XL-A/I rotor chamber completely above the rotor. There are two new features in this setup: first, the laser excitation light comes from outside via a glass fiber into the vacuum rotor chamber and, second, the light does not penetrate the complete measuring cell. Rather, only the back-scattered fluorescence light is measured by step-wise radial scanning of the whole surface of the cell along a sector. This is reached by a confocal setup of the detector geometry [12]. Figure 5.12 shows a measurement with Laue's fluorescence detector.

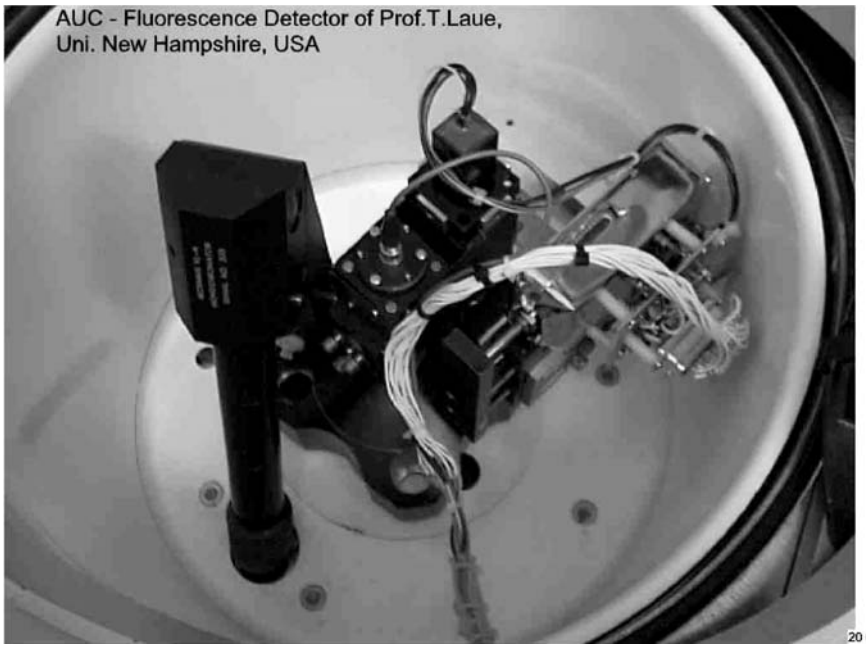

Fig. 2.12. Photograph of a user-made fluorescence detector realized by Laue [12] inside a XL-A/I vacuum chamber (reprinted with permission from [12])

Turbidity Detectors

Similarly to the case of the fluorescence detector, to our knowledge there are just two types of turbidity (= light scattering) detectors [13, 14]. Both are user-made, and therefore not commercially available. However, it is not very difficult to build such a turbidity detector. Again, only a short description is given here.

The principle of a turbidity measurement is comparable to that of an absorption detector, but it is much simpler, because the absorption $A = \lg(I_0/I)$ is measured at only one fixed radial position r_{slit}. Figure 2.13 shows a schematic diagram of the turbidity detector developed at BASF, which is part of a particle sizer.

The turbid dispersion to be analyzed is diluted to about $c = 1\,\text{g/l}$, and placed into the centerpiece of the 3-mm mono-sector cell. In the first version of the BASF turbidity detector [13], the lower quartz window of the cell is covered by an apertured stop, in the center of which is a 0.2 mm wide slit arranged perpendicularly to the radius of the rotor. The slit picks out a beam from the entering parallel monochromatic light. This is simply created by using a stabilized incandescent lamp as a light source, and a monochromatic light filter ($\lambda = 546\,\text{nm}$) after the condensing lens.

The intensity I of the beam, which is reduced by light scattering of the latex particles inside the measurement cell, according to Mie's light scattering theory, is registered by the photomultiplier and recorded as a function of the running time t. The concentration c of the dispersions is selected so as to yield an initial light intensity $I_{t=0} = I_0$ of approximately 10% of $I_{t=\infty} = I_{\text{DM}}$, the intensity of the pure dispersant, reached at the end of the run.

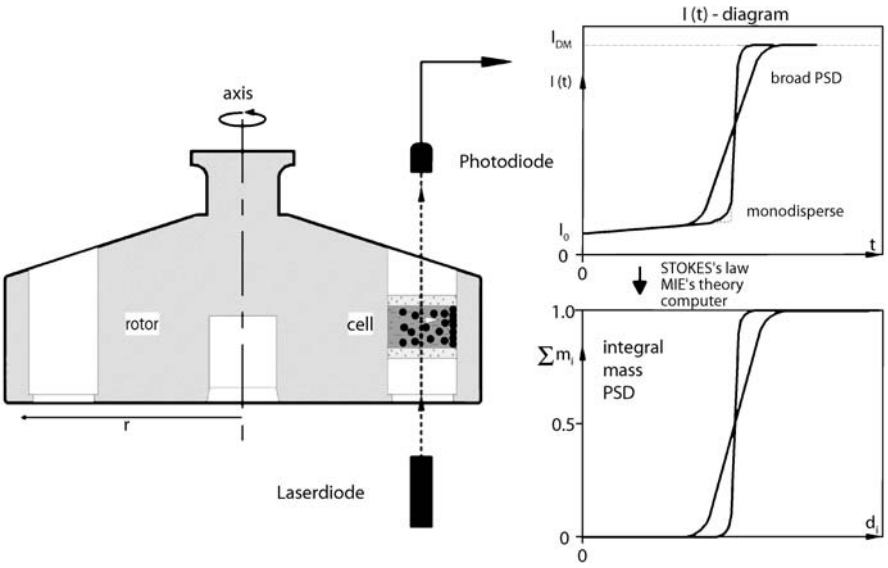

Fig. 2.13. Schematic setup of a user-made particle sizer with a turbidity detector to measure particle size distributions; realized in the AUC laboratory at BASF

A second (newer) version of the turbidity detector in use today [5] applies a narrow continuous light beam of a laser diode ($\lambda = 670\,\text{nm}$) with 0.2 mm diameter, no apertured stop, and a fast photodiode as light detector (see Fig. 2.13).

In the case of a monodisperse latex, all of the particles sediment with exactly the same velocity. This causes a sharp one-step $I(t)$ curve to be obtained (shown in Fig. 2.13), because the intensity jumps from $I_{t=0}$ to I_{DM} at the moment when the sharply defined, sedimenting latex front passes the measuring slit (or the laser beam). The diameter d_{p} of the monodisperse particles can be calculated from the measured jump time t by means of Stokes' law (1.9). In the case of a broadly distributed latex, fractionation by particle size results in a broad $I(t)$ curve (shown in Fig. 2.13) because of large particles running ahead and small particles lagging behind. Details of this particle size distribution measuring procedure, in particular for very broadly distributed particles, are given in Sect. 3.6. Although a mono-sector cell is used, $I(t)$ and I_{DM} can be measured in the same run, and thus the time-dependent absorption $A(t) = \lg(I_{\text{DM}}/I(t))$ at the radius position r_{slit} can be calculated. Figure 2.14 shows a picture of the newest turbidity detector with a thin green laser beam as realized recently at BASF. This green laser light ($\lambda = 546\,\text{nm}$) enters from the outside via a glass fiber into the vacuum rotor chamber of the Optima XL.

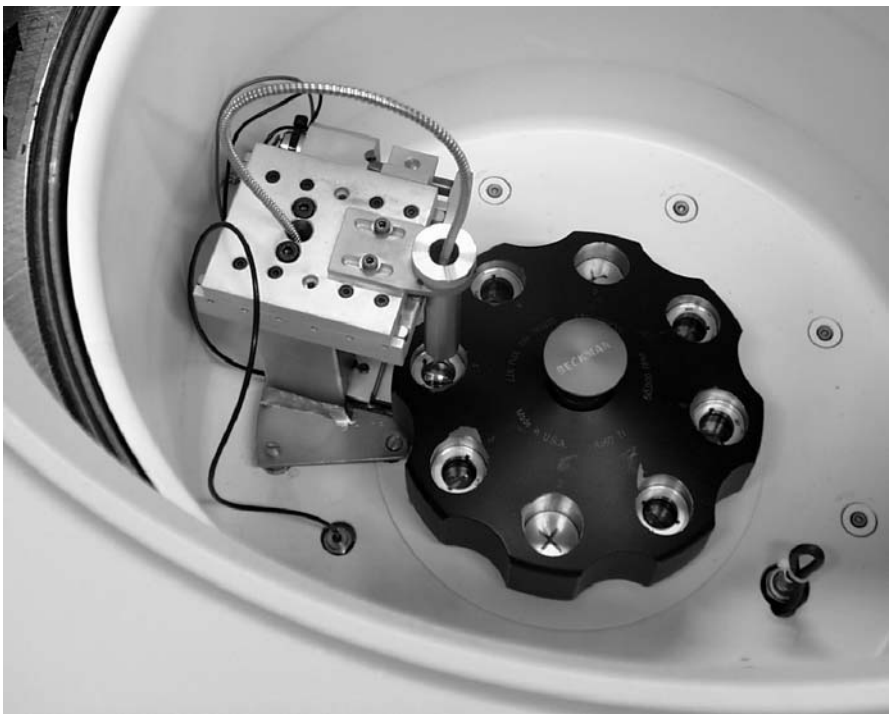

Fig. 2.14. Photograph of the turbidity detector system with a thin green laser beam realized in the AUC laboratory at BASF, inside the vacuum chamber of an Optima XL for measuring of particle size distributions; the glass fiber guiding the laser light from outside is visible

2.5 Multiplexer

A pronounced improvement of all kinds of AUC measurements was reached when a multiplexer unit was added to analytical ultracentrifuges. This allowed the measurement of not just one but up to seven samples in an eight-hole rotor in one and the same experimental run. Thus, the effectiveness of the AUC is increased by a factor of 7. In this section, we describe the homemade multiplexer as realized in the Schlieren optical system described in Sect. 2.4.3.

In contrast to earlier multiplexer developments [20, 21], the system is now completely automated. The software-based multiplexer is realized via a Lab-view-based software tool applying a NIDAQ-Board (National Instruments, Austin, USA).

The triggering signal is created by the following homemade system. A photoelectric reflection light gate is fixed to the bottom of the vacuum chamber. This reflection gate consists of a continuously light-emitting LED and a fast photodiode. A "mirror" (= a polished small strip at the rotor bottom) fitted on the base of the analytical rotor reflects the light of the LED. By this alignment, each revolution of the rotor generates one sharp electrical pulse. This signal is imported by the data acquisition software, and used for the calculation of the actual rotor speed and for the calculation of the actual cell positions. The pulse-times of the flash lamp to ensure illumination of the desired superimposed cells are calculated from these data.

2.6 Auxiliary Measurements

As mentioned in preceding sections, a few auxiliary parameters have to be known to interpret sedimentation velocity data (and equilibrium run data, too; see Sect. 5.2). These are the density of the solvent ϱ_s, the viscosity of the solvent η_s, and the particle density ϱ_p or its reciprocal, the partial specific volume of the solute $\overline{v} = 1/\varrho_p$. Furthermore, for detection of the solute/particle concentration c in sedimentation experiments by Schlieren, turbidity, UV absorption or interference optics, the following optical parameters are required: refractive indices of the solvent and the solute/particle, n_s and n_p, respectively, the specific refractive index increment of the solute $(dn/dc)_p$ or the specific decadic absorption coefficient ε according to Lambert–Beer's law. Most of these parameters can be found in table-works [22,23], or need only simple measurements, such as for η_s with capillary viscometers, or ε with UV spectrometers (the XL-A/I itself is a UV spectrometer!). The measurements of the two most important AUC parameters, $\overline{v} = 1/\varrho_p$ and $(dn/dc)_p$, are presented in the two following sections.

2.6.1 Measurement of the Solvent Density and the Partial Specific Volume

As mentioned above, the partial specific volume $\bar{v}$ is the inverse of the solute/particle density ϱ_p. The partial specific volume $\bar{v}$ is defined as the volume increase obtained if 1 g of solute is added to an infinite amount of solvent. Precise knowledge

of this parameter is crucial for the interpretation of sedimentation data. This is because of the small differences in the buoyancy term $(1 - \bar{\nu} \cdot \varrho_s)$. In fact, it is the most common hindrance for the even more universal use of analytical ultracentrifugation in physicochemical science. Therefore, a lot of work has been spent on this topic, which led to extensive tabulated data of synthetic polymers and biopolymers. For proteins – as mentioned above, they are still the most common materials analyzed in analytical ultracentrifuges today – it is possible to estimate the value of $\overline{v} = 1/\varrho_p$ because this often does not deviate too much from approximately $0.73\,cm^3/g$.

The best way to measure $\varrho_p = 1/\overline{v}$ is by using the well-known Kratky density balance. Figure 2.15 shows a measuring example. For the pure solvent and for ca. three solutions with different concentrations c of the solute, the (absolute) densities ϱ are measured (these solutions can also be used to determine the $(dn/dc)_p$ of the solute as well; see following section). Then, the reciprocal of ϱ, the specific volume $v = 1/\varrho$, is plotted as function of c. The slope of a regression line yields the wanted value of $\bar{\nu} = (\varrho_p)^{-1}$ of the solute. The example presented in Fig. 2.15 is a polybutyl acrylate latex dispersed in water at 25 °C. The results of this plot are $\varrho_p = 1.048\,g/cm^3$ and $\overline{v} = 0.954\,cm^3/g$.

Another important possibility to determine the solute density ϱ_p will be subject of Chap. 4: the determination of particle densities in AUC density gradients.

The use of a pycnometer is also possible, but tedious. Furthermore, a classical method to determine solution densities is the use of calibrated sinkers/floaters that make use of the Archimedes principle. Edelstein and Schachman [24] determined for special cases the partial specific volume by variation of solvents. They measured the product $M(1 - \bar{\nu} \cdot \varrho_s)$, called the effective molar mass, in different solvents with varying known densities, such as H_2O and D_2O, using equilibrium runs (see Chap. 5). The partial specific volume $\overline{v}$ can then be computed from these data. In a similar manner, Lustig et al. [25] and Schubert et al. [26] worked with Nycodenz/water solutions of different compositions, respectively, with two solvents

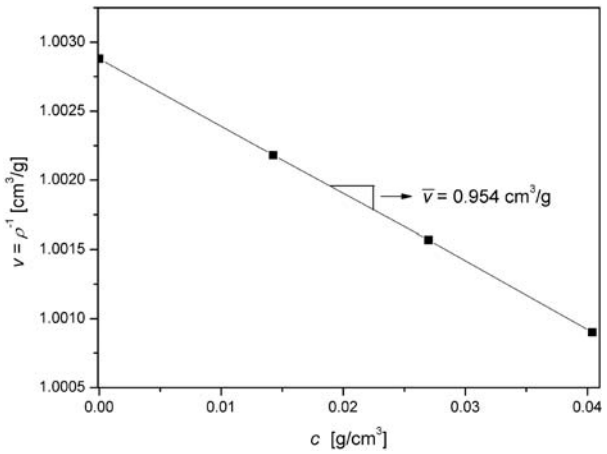

Fig. 2.15. $1/\varrho - c$ plot to determine the partial specific volume $\bar{\nu} = 1/\varrho_p$ from measurements with a Kratky density balance (polybutyl acrylate latex, water, 25 °C)

of very different densities and some mixtures thereof (see Sect. 5.4.2). A known table-work for $\overline{v}$ values of biopolymers is [27].

2.6.2 Measurement of the Refractive Index and the Specific Refractive Index Increment

In order to measure n_s, n_p and the specific refractive index increment $(dn/dc)_p$ of dissolved macromolecules and dispersed particles, often a Bellingham-refractometer is applied. It allows the measurement at just one wavelength λ. Usually, solutions of the solute of ca. three different concentrations are prepared. It is favorable to use the same solutions that have been prepared to determine the solute density (see Sect. 2.6.1). The (absolute) values of the measured refractive indices n of the pure solvent and the solutions are then plotted as function of c (see Fig. 2.16). The intercept yield n_s and the slope of the resulting line gives the specific refractive index increment $(dn/dc)_p$, that is, the change of the refractive index of the solution per unit mass solute that has been added. The result of this plot is $(dn/dc)_p = 0.130\,cm^3/g$ (for the same polybutyl acrylate latex as in Fig. 2.15, 25 °C, 589 nm). Well-known $(dn/dc)_p$ table-works are [23] for synthetic polymers, and [28] for biopolymers.

If more detailed information at different wavelengths λ is required, a differential refractometer should be applied. It should be mentioned that the refractive index n, and thus $(dn/dc)_p$, varies with the wavelength λ and with the temperature T.

For *PSD* measurements, using a turbidity detector and Mie's theory, instead of $(dn/dc)_p$, the (absolute) refractive index n_p of the dispersed particles is required. Equation (2.4) gives a formula that allows the roughly approximated calculation of n_p using the measured $(dn/dc)_p$, and vice versa.

$$n_p = (dn/dc)_p \cdot \varrho_p + n_s \tag{2.4}$$

This equation was derived making use of the additivity of molar refractions [29].

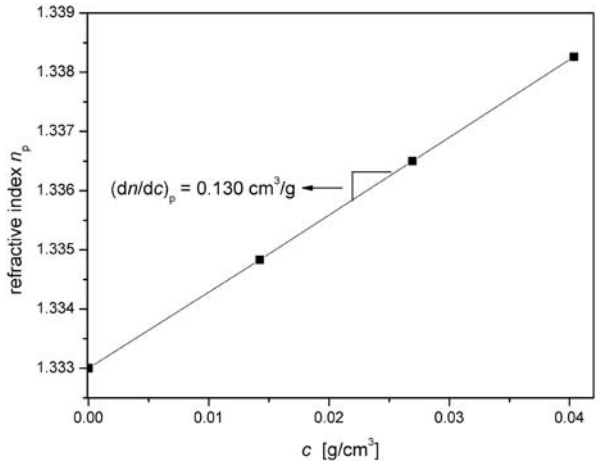

Fig. 2.16. $n - c$ plot to determine the specific refractive index increment $(dn/dc)_p$ from measurements with a Bellingham refractometer (polybutyl acrylate latex, water, 25 °C, 589 nm)

References

1. Svedberg T, Pedersen KO (1940) Die Ultrazentrifuge. Steinkopff, Dresden
2. http://www.ehs.cornell.edu
3. Bowen TJ, Rowe AJ (1970) An introduction to ultracentrifugation. Wiley, London
4. Lewis MS, Weiss GH (1976) Proc Conf Fifty Years of the Ultracentrifuge, 24–26 February 1975, Bethesda, ML, Biophys Chem 5:1–286
5. Mächtle W (1999) Biophys J 76:1080
6. Müller HG (1999) Bayer AG, Leverkusen, Germany, personal communication
7. Mächtle W (1999) Prog Colloid Polym Sci 113:1
8. Börger L, Lechner MD, Stadler M (2004) Prog Colloid Polym Sci 127:19
9. Schachman HK (1959) Ultracentrifugation in biochemistry. Academic Press, New York
10. Lloyd PH (1974) Optical methods in ultracentrifugation, electrophoresis and diffusion. University Press, Oxford
11. Schmidt B, Riesner D (1992) In: Harding SE, Rowe AJ, Horton JC (eds) Analytical ultracentrifugation in biochemistry and polymer science. The Royal Society of Chemistry, Cambridge, p. 176
12. MacGregor IK, Anderson AL, Laue TM (2004) Biophys Chem 108:165
13. Mächtle W (1984) Makromol Chem 185:1025
14. Scholtan W, Lange H (1972) Kolloid Z Z Polym 250:782
15. Mächtle W (1991) Prog Colloid Polym Sci 86:111
16. Böhm A, Kielhorn-Bayer S, Rossmanith P (1999) Prog Colloid Polym Sci 113:121
17. Billick IH, Bowen RJ (1965) J Phys Chem 69:4024
18. Furst A (1997) Eur Biophys J 25:307
19. Rossmanith P, Mächtle W (1997) Prog Colloid Polym Sci 107:159
20. Mächtle W, Klodwig U (1976) Makromol Chem 177:1607
21. Mächtle W, Klodwig U (1979) Makromol Chem 180:2507
22. Lide DR (ed) (2002) CRC handbook of chemistry and physics, 83rd edn. CRC Press, Boca Raton
23. Brandrup J, Immergut EH (eds) (1989) Polymer handbook, 3rd edn. Wiley, New York
24. Edelstein SJ, Schachman HK (1967) J Biol Chem 242:306
25. Lustig A, Engel A, Tsiotis G, Landau EM, Baschong W (2000) Biochim Biophys Acta 1464:199
26. Tziatzios C, Precup AA, Lohmeijer BGG, Börger L, Schubert US, Schubert D (2004) Prog Colloid Polym Sci 127:54
27. Durchschlag H (1986) In: Hinz HJ (ed) Thermodynamic data for biochemistry and biotechnology. Springer, Berlin, Heidelberg, New York, pp. 45–128
28. Theisen A, Johann C, Deacon MP, Harding SE (2000) Refractive increment data book for polymer and biomolecular scientists. Nottingham University Press, Nottingham
29. Mächtle W, Fischer H (1969) Angew Makromol Chem 7:147
30. Ralston G (1993) Introduction to analytical ultracentrifugation. Beckman Instruments, Fullerton, CA
31. Gonzales JM, Rivas G, Minton AP (2003) Anal Biochem 313:133

http://www.springer.com/978-3-540-23432-6

Analytical Ultracentrifugation of Polymers and Nanoparticles

Maechtle, W.; Börger, L.

2006, XIII, 237 p., Hardcover
ISBN: 978-3-540-23432-6